PRAMANA
— journal of
physics

Vol. 67, No. 1
July 2006
pp. 33–46

Order and chaos in soft condensed matter

A K SOOD and RAJESH GANAPATHY
Department of Physics, Indian Institute of Science, Bangalore 560 012, India
E-mail: asood@physics.iisc.ernet.in

Abstract. Soft matter, like colloidal suspensions and surfactant gels, exhibit strong response to modest external perturbations. This paper reviews our recent experiments on the nonlinear flow behaviour of surfactant worm-like micellar gels. A rich dynamic behaviour exhibiting regular, quasi-periodic, intermittency and chaos is observed. In particular, we have shown experimentally that the route to chaos is via Type-II intermittency in shear thinning worm-like micellar solution of cetyltrimethylammonium tosylate where the strength of flow-concentration coupling is tuned by the addition of sodium chloride. A Poincaré first return map of the time series and the probability distribution of laminar length between burst events show that our data are consistent with Type-II intermittency. The existence of a 'Butterfly' intensity pattern in small angle light scattering (SALS) measurements performed simultaneously with the rheological measurements confirms the coupling of flow to concentration fluctuations in the system under study. The scattered depolarised intensity in SALS, sensitive to orientational order fluctuations, shows the same time-dependence (like intermittency) as that of shear stress.

Keywords. Surfactants; stress relaxation; flow instabilities; rheo-optics.

PACS Nos 82.70.Uv; 83.85.St; 83.85.Ei; 82.70.Gg; 83.60.Wc

1. Introduction

Soft condensed matter (SCM) systems are ubiquitous in nature. Colloidal suspensions, surfactant gels and polymeric systems are just a few examples [1]. Soft matter is middle ground between two extremes: the fluid state, where thermal fluctuations are very important, and the solid state. However diverse these systems are, they share certain common features: (i) The constituents that make up soft matter are large polyatomic structures. The focus is not on atomic details and a coarse grained approach is taken in understanding these materials. (ii) Self-organisation is a very important feature of these systems. The polyatomic molecules self-assemble to form large heterostructures on changing either their concentration or increasing/decreasing temperature. For example, on changing the concentration of the amphiphilic molecules, one can go from monomers to micelles to cubic/hexagonal/lamellar phases. (iii) These materials show strong response to modest external perturbations like shear flow, electric, magnetic and gravitational fields and hence are interesting candidates for the study of non-equilibrium phenomena. (iv) These materials are weakly connected and have low density. The

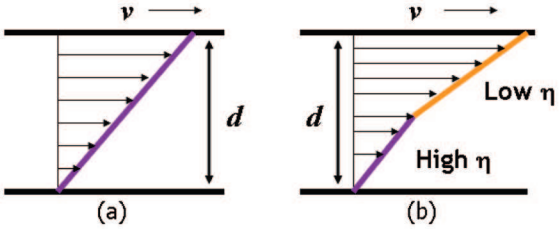

Figure 1. Schematic of a Couette flow between two parallel plates. (**a**) Homogenous flow and (**b**) shear banded flow. The arrows indicate the magnitude of the flow velocity.

elastic constants are very low compared to atomic systems. For example, a colloidal gel/crystal has typical elastic modulus ∼10 Pa whereas the elastic modulus of steel is $\sim 10^{12}$ Pa [2–4].

The effect of shear flow on these materials has aroused immense interest in recent times. Figure 1a shows a schematic of the planar Couette flow arrangement [5], one of the standard ways to apply shear. The material of interest is held between two parallel plates separated by a distance d and the top plate is moved with a velocity v while the bottom plate is held fixed. The shear rate $\dot{\gamma}$ is given by, $\dot{\gamma} = v/d$. Shear has units of 1/s and hence $\tau_{\rm Shear} = 1/\dot{\gamma}$ is the time-scale set by the shear flow. The typical relaxation time of stress, $\tau_{\rm Relax}$, in soft materials is 10^{-3} s, unlike conventional solids where the relaxation time $\tau_{\rm Relax} \sim 10^{-12}$ s. The large relaxation time of SCM systems imply that $\dot{\gamma}\tau_{\rm Relax} \sim 1$ can be achieved in these systems. Thus in SCM systems shear flow is coupled to the microstructure unlike conventional solids, where one needs to apply incredibly large shear rates that are unattainable in a typical experiment before one sees such a coupling. It is useful to define a dimensionless number called the Peclet number P_e given by $P_e = \tau_{\rm Diff}/\tau_{\rm Shear}$ where, $\tau_{\rm Diff}$ is the Brownian diffusion time and is given by $\tau_{\rm Diff} \sim 6\pi\eta a^3/k_{\rm B}T$. Here a is the radius of the macromolecule, η is the viscosity, $k_{\rm B}$ is the Boltzmann constant and T is the temperature. If $P_e \ll 1$ (i.e. $\tau_{\rm Diff} \ll \tau_{\rm Shear}$), Brownian motion is able to maintain an unperturbed state. If $P_e \gg 1$ implying $\tau_{\rm Diff} \gg \tau_{\rm Shear}$, the shear flow modifies the structure and Brownian motion is unable to restore structure on a time-scale set by the shear rate.

The main focus of this article is our ongoing study of worm-like micellar gels of surfactant cetyltrimethylammonium tosylate which shows a rich dynamic behaviour under shear flow.

2. Surfactants

Surfactants are amphiphilic molecules comprising of a polar head group and a hydrophobic long chain hydrocarbon tail [6]. This amphiphilic nature of the molecule gives rise to a variety of phases in an aqueous medium since the polar head group prefers to stay in water whereas the hydrocarbon tail tries to shield itself from water. In a polar solvent at very low concentrations, they exist as monomers. On increasing the surfactant concentration beyond critical micellar concentration

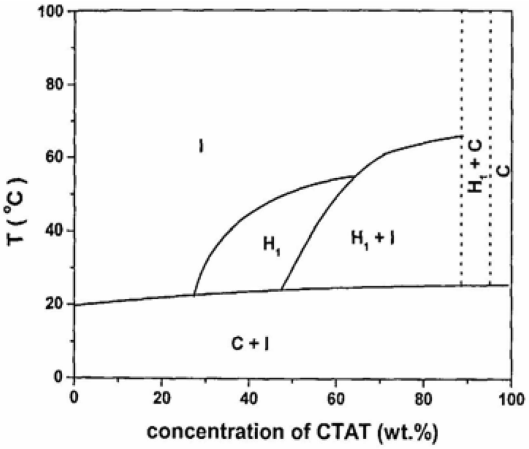

Figure 2. Phase diagram of CTAT [8]. I: Isotropic phase, H: hexagonal phase and C: cubic phase.

(CMC), they form spherical micelles with the polar head groups pointing out and tails pointing in. At higher concentrations, these spherical micelles can elongate to form long flexible cylindrical micelles which above the overlap concentration c^* entangle to form viscoelastic gels [7]. At very high concentrations they can form ordered phases like hexagonal, cubic and lamellar phases. The phase behaviour of the cationic surfactant CTAT has been well-characterised by Soltero *et al* [8] (figure 2). Above the Krafft temperature of 23°C and at concentrations 0.04 wt% $< c <$ 0.4 wt% cylindrical micelles are formed which, at $c > c^* = 0.4$ wt%, entangle to form viscoelastic gels.

3. Experimental

The CTAT/water and CTAT/NaCl/water samples were prepared by dissolving known amounts of CTAT (formula wt: 455.7, Sigma Aldrich) in water and brine, respectively, and this study mainly focuses on the latter. The samples were filtered through 200 nm pore size filters to remove dust impurities and left to equilibrate for two days. The experiments were carried out on a MCR 300 stress-controlled rheometer (Anton PAAR, Germany) with small angle light scattering attachment (SALS) at a temperature of 26.5°C (figure 3). The rheometer is intrinsically stress-controlled and was used in the feedback mode for strain-controlled experiments. All experiments were carried out in a cylindrical Couette geometry with top and bottom windows made of quartz glass (inner cylinder diameter 32 mm, height 16.5 mm and gap 2 mm). A vertically polarised (V) laser beam ($\lambda = 658$ nm and spot size = 1 mm) enters the gap between the cylinders (the beam is close to the inner rotating cylinder and cannot be translated across the gap) along the vorticity ($\nabla \times v$) direction, where v is the velocity field. An analyser below the Couette geometry allows us to select either the vertically (referred as VV) or the horizontally polarised (referred as VH) scattered light from the sample without disturbing

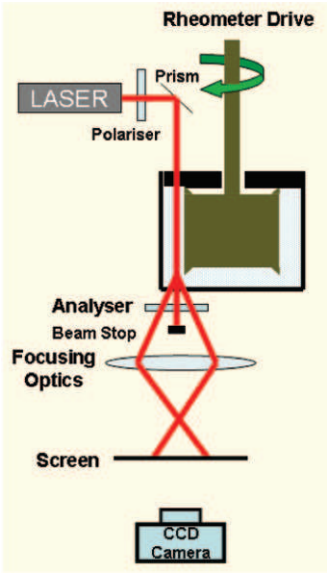

Figure 3. Schematic of the rheo-small angle light scattering set-up.

the measurements. A condenser beneath the analyser collects the scattered light dominantly from a plane 6 mm above the bottom plate and forms the image on a screen in the $(v, \nabla v)$ plane. The imaging was done using a 8-bit colour CCD camera (Lumenera 075C, 640 × 480 pixels, maximum frame rate = 60 fps) at a frame rate of 1 frame/750 ms. About 3000 images were grabbed for each polarisation while stress relaxation measurements were simultaneously going on. The intensity at various wave vectors from the noise filtered image was measured and a time series was generated by repeating the process over each image.

4. Background

In a linear rheology experiment, one studies the response of a material to very small stresses (i.e. small compared to the thermal fluctuations in the material) [9]. Nonlinear rheology describes the response of a material to large stresses and it is in this regime one sees novel flow behaviour [5]. As the name suggests, the strain developed in the sample changes nonlinearly with the applied stress in this regime. The nonlinear flow behaviour is characterized by shear thinning or thickening, the presence of non-zero yield stresses and normal stress differences, flow-induced phase transitions and the phenomenon of shear banding. Systems of giant worm-like micelles formed in certain surfactant solutions are known to show very unusual nonlinear rheology. In a controlled stress measurement of the flow curve the stress is known to saturate beyond a critical shear rate, while the first normal stress difference increases roughly linearly with shear rate. Cates and coworkers were the first to predict this kind of flow behaviour and they attribute this to a mechanical instability of the

shear banding type [10]. In shear banding systems, the system splits into coexisting bands that support the same stress but have different average shear rates (figure 1b). The high shear rate band is lower in viscosity and is the nematic phase, while the low shear band has a higher viscosity and is the isotropic phase. This kind of behaviour may be understood in terms of the reptation-reaction model which involves the reversible breakage and recombination of worm-like micelles along with reptation dynamics known for polymer solutions. The flow curve can be measured under controlled stress or strain rate and depending on the time interval between the collection of data points, we can obtain metastable or steady state branches, respectively.

In shear thinning worm-like micellar solutions of surfactant cetyltrimethylammonium tosylate (CTAT) that shows a plateau in the flow curve, Bandyopadhyay *et al* found interesting time dependence in the relaxation of the stress and normal force in step shear rate experiments for shear rate values fixed in the plateau region [11]. A time series analysis of the stress data using the delay-embedding method, done using the TISEAN software [12], showed the existence of a positive Lyapunov exponent, a measure of divergence of trajectories in phase space, and a fractal correlation dimension >2 implying that the signal was chaotic rather than the stochastic noise. This has led to many theoretical [13–17] and experimental studies of this striking effect, termed as 'rheochaos', in a wide variety of other systems including shear-thickening worm-like micellar solutions [18], lamellar, onion and sponge phases of surfactants [19] and dense colloidal suspensions [20]. NMR velocimetry and rheo-optical experiments suggest that rheochaos is closely linked to the phenomenon of shear banding [21]. These experiments have shown that the interface between the shear rate bands is not stable as predicted [10], but shows complex spatio-temporal dynamics and this is accompanied by stress/shear rate fluctuations. Spatial heterogeneity should play a role in understanding rheochaos as exploited in recent theoretical models [22,23].

These experiments raised three important questions that have remained unaddressed in experimental literature so far:

1. What is the route to rheochaos?
2. Does a concentration difference between the shear bands affect rheochaos?
3. What is the role played by the nematic alignment of the worm-like micelles on rheochaos?

There are primarily three routes to chaos: the period-doubling route, the quasi-periodic route and the intermittency route. The intermittency route is mainly characterised by bursts of chaos disrupting nearly periodic (laminar region) oscillations. Pomeau and Manneville [24] have established that within the intermittency route there are further three types. Type-I appears with an inverse tangent bifurcation, Type-II with a Hopf bifurcation and Type-III is associated with a period doubling bifurcation. Experimentally, all three types of intermittency have been observed in a variety of hydrodynamical and electrical systems [25], although there are fewer examples of Type-II intermittency which sets in via quasi-periodicity. Our experiments, we show below, are consistent with Type-II intermittency route to chaos.

5. Motivation

In a recent theoretical study, Fielding and Olmsted [26] have taken into account the effect of concentration coupling in shear banding worm-like micellar systems that are far from zero-shear isotropic–nematic (I–N) transition. Their d-JS-ϕ model (spatially non-local Johnson–Segalman model with concentration coupling) calculations predict a positive value for the slope of the plateau in the banded region of the flow curve, and the slope increases with the strength of the coupling between flow and concentration fluctuations (figure 4). In a recent experimental work, Bandyopadhyay and Sood [27] have shown that the slope α of the stress plateau, which we find is a power law $\sigma \sim \gamma^{\alpha}$, for worm-like micellar solutions of surfactant cetyltrimethylammonium tosylate (CTAT) can be tuned by adding salt (NaCl) (figure 5).

These results motivated us to study the consequences of flow-concentration coupling on the stress relaxation dynamics in this class of systems.

6. Results and discussion

Figure 6a (filled circles) shows the flow curve for CTAT 2 wt% in a controlled-stress experiment. The flow curve shows a near-plateau for $\dot{\gamma} > 0.1$ s^{-1}. The observed weak departure (slope $\alpha = 0.07$ in the log–log plot) from a true plateau is very likely due to the small inhomogeneity of the stress field arising from curvature effects in the cylindrical Couette geometry [26]. The increase in stress due to geometry curvature alone has been calculated using the relation:

$$\frac{\Delta\sigma}{\sigma} = \frac{2\Delta R}{R}. \tag{1}$$

Here, $\Delta\sigma$ is the increase in stress across the plateau due to cell curvature, σ is the stress at the plateau onset, ΔR is the gap between the cylinders and R is the radius

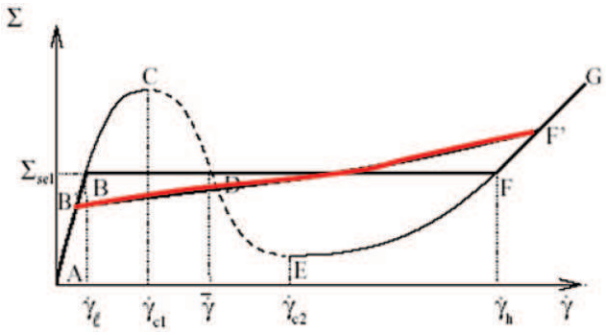

Figure 4. Theoretical prediction for a system showing flow-concentration coupling. The red line B′F′ is when the shear bands have different concentrations. The line BF is for a system that does not show a concentration difference between the shear bands [26].

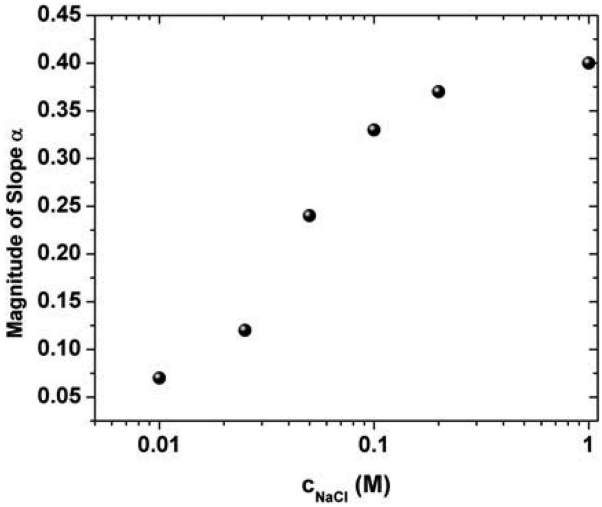

Figure 5. Magnitude of slope of the flow curve plotted against NaCl concentration for CTAT surfactant concentration of 2 wt%.

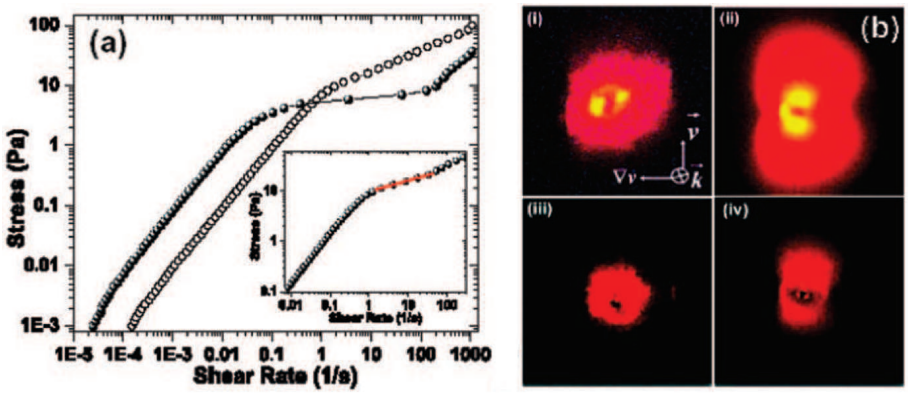

Figure 6. (**a**) Flow curves for CTAT 2 wt% (solid circles) and CTAT 2 wt% + 100 mM NaCl (hollow circles). Inset: Flow curve for CTAT 2 wt% + 50 mM NaCl. (**b**) SALS profiles for (i) and (iii) CTAT 2 wt% for VV and VH polarizations and (ii) and (iv) CTAT 2 wt% + 100 mM NaCl for VV and VH polarizations [30].

of the inner cylinder. The increase in stress calculated using (1) is 1.6 Pa for pure CTAT 2 wt% which is in good agreement with the experimental value of ∼1.3 Pa.

Figure 6a also shows the flow curve for CTAT 2 wt% + 100 mM NaCl (hollow circles). The stress shows a much stronger shear rate dependence ($\alpha = 0.32$ for CTAT 2 wt% + 100 mM NaCl and $\alpha = 0.24$ for CTAT 2 wt% + 50 mM NaCl; see figure 6a, inset) above $\dot{\gamma} > 1\ \mathrm{s}^{-1}$ which cannot be due to geometry effects alone. We attribute this slope to a concentration difference between the shear rate bands [22,26]. Berret *et al* [23] found similar values of slope for the system CpCl/hexanol/NaCl

for concentrations just below the I–N coexistence concentration of 32 wt%. Our system is in the semi-dilute region and is far from a zero-shear I–N transition ∼27 wt% for pure CTAT and >30 wt% for CTAT + 50 mM NaCl. Hence, a large slope α is not due to I–N coexistence. A concentration difference between the shear rate bands can arise from a Helfand–Fredrickson mechanism [28]. In a sheared micellar solution, the portion of the micelle mired in the low viscosity shear band, on relaxing will move more than the micelle trapped in the high viscosity region. Hence on average the molecule moves towards the low shear rate band. This mechanism provides a positive feedback whereby micelles can move up their own concentration gradients and thereby lead to flow-enhanced concentration fluctuations. The high shear rate band is predicted to be lower in concentration than the low shear rate band. If so, our SALS experiments should show a 'Butterfly' light scattering pattern with the wings of the butterfly stretched along the flow direction [29]. Figure 6b shows the SALS pattern in VV geometry for CTAT 2 wt% and CTAT 2 wt% + 100 mM NaCl. The 'Butterfly' pattern is absent for the pure CTAT 2 wt% (figure 6b(i)) and is present for CTAT 2 wt% + 100 mM NaCl (figure 6b(ii)) and (iii) and (iv) in figure 6b show corresponding patterns in VH geometry. We have carried out experiments at six different salt concentrations 10 mM $< c_{\mathrm{NaCl}} <$ 1 M, which yield plateau slopes ranging from $0.07 < \alpha < 0.4$ (figure 5). We find that a minimum slope of 0.12, corresponding to a salt concentration of 25 mM NaCl, is essential to see a 'Butterfly' pattern indicating the onset of flow-concentration coupling at this α value [30].

Figures 7a–e show the stress relaxation dynamics for various shear rates fixed in the plateau region for the system CTAT 2 wt% + 100 mM NaCl. At a $\dot{\gamma} = 0.05$ s^{-1} the stress does not show any dynamics. As the shear rate is increased to $\dot{\gamma} = 10$ s^{-1}, the stress oscillations look periodic (figure 7b). At $\dot{\gamma} = 20$ s^{-1} the system shows oscillations with two modes that appear twice during the course of the experiment. Figure 7d shows the stress relaxation dynamics at $\dot{\gamma} = 23$ s^{-1}, The signal looks periodic, but a closer inspection reveals finer features that do not repeat exactly. Figure 8 shows the power spectrum of this signal. Apart from the two primary frequencies centered around $\omega_1 = 0.049$ Hz and $\omega_2 = 0.061$ Hz and their higher harmonics, there are other frequency components centered at linear combinations of ω_1 and ω_2 like $\omega_2 - \omega_1$ and $\omega_2 + \omega_1$. These extra features are hallmark of a 2-frequency quasiperiodic signal [31]. In figure 7e, there are bursts of chaos breaking in between the quasiperiodic signal $\dot{\gamma} = 25$ s^{-1}. The power spectrum of the quasiperiodic laminar region once again shows two frequencies centered around $\omega_1 = 0.057$ Hz and $\omega_2 = 0.063$ Hz, implying a decrease in the time period with increasing shear rate. The stress relaxation dynamics at $\dot{\gamma} = 27.5$ s^{-1} (figure 7f) was completely chaotic (characterised by a positive Lyapunov exponent ∼0.14 and an exponential Fourier power spectrum [32]). Although the exact shear-rate values at which the sample displayed the above features was found to differ to some extent from run to run, the main features, namely, quasiperiodic oscillations and intermittent bursts were found in all the runs. We do not observe any quasiperiodic and intermittent behaviour for CTAT 2 wt% (figure 9a–e) and CTAT 2 wt% + 10 mM NaCl, which have $\alpha < 0.12$, for different shear-rate histories. All systems with $\alpha > 0.12$, implying moderate to strong flow-concentration coupling, showed quasiperiodicity and intermittency [30].

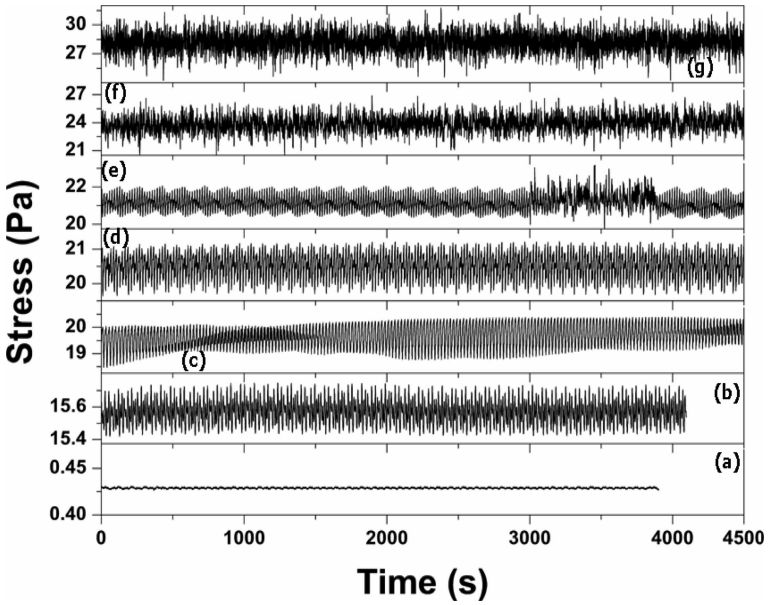

Figure 7. Stress relaxation at various shear rates for CTAT 2 wt% + 100 mM NaCl. (**a**) 0.05 s^{-1}, (**b**) 10 s^{-1}, (**c**) 20 s^{-1}, (**d**) 23 s^{-1}, (**e**) 25 s^{-1}, (**f**) 27.5 s^{-1} and (**g**) 40 s^{-1}.

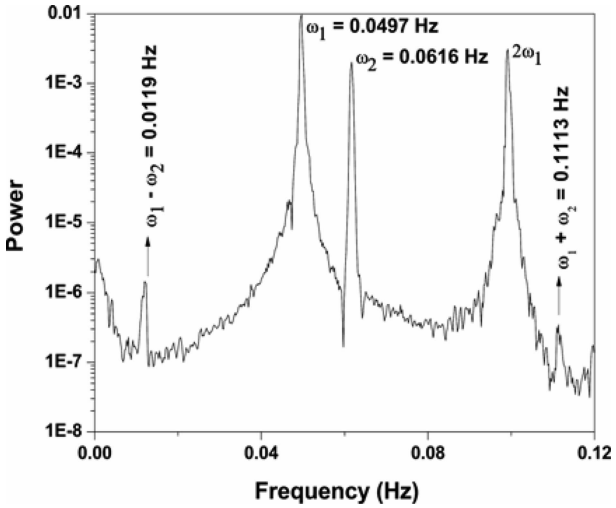

Figure 8. Fourier power spectrum for the time series shown in figure 7d.

Figure 10a shows the partial time series at $\dot{\gamma} = 22\ s^{-1}$ obtained during a different run. Judging by the nature of the signal during the laminar phase, Type-III intermittency can be ruled out, since, for this type of intermittency there is a subharmonic mode with increasing amplitude. We follow the method described by

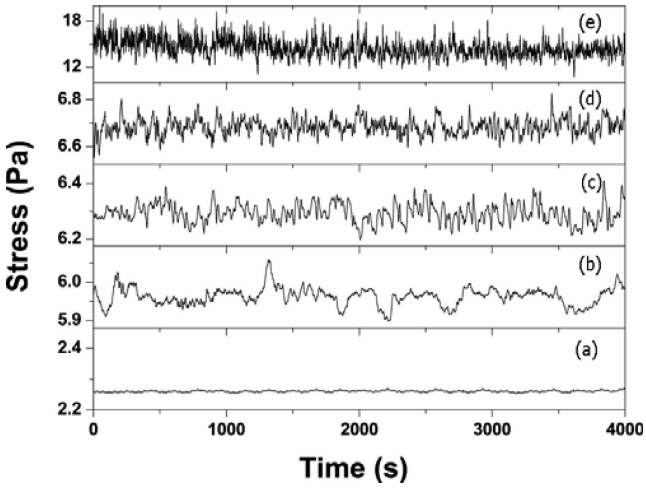

Figure 9. Stress relaxation at various shear rates for CTAT 2 wt%. (**a**) 0.05 s^{-1}, (**b**) 10 s^{-1}, (**c**) 20 s^{-1}, (**d**) 40 s^{-1} and (**e**) 300 s^{-1}.

Berge *et al* [33] and reconstruct a Poincaré plot by taking the successive minima of the stress in the laminar region after a chaotic burst. In figure 10c, we plot the value of the stress at the Nth minimum against its value at the $(N-1)$th minimum. This plot exhibits a spiraling behaviour characteristic of Type-II intermittency. The spiraling behaviour is time inverted and we call this time inverted Type-II intermittency after Sacher *et al* who found similar behaviour in a semiconductor laser with external feed back [34]. The above behaviour implies that the system oscillates back to the laminar phase after a disturbance that caused a burst event. A standard test for Type-II intermittency is the probability distribution of laminar lengths L between burst events that scales as $P(L) \sim L^2$ for small times and shows an exponential tail at larger times [35]. Due to an insufficient number of burst events, this test could not be carried out for the above-mentioned time series. In figure 10b we show the time series obtained for CTAT 2 wt% + 50 mM NaCl ($\alpha = 0.24$) at $\dot{\gamma} = 19$ s^{-1} which shows about fifty bursts in a 2 h run. The probability distribution of laminar lengths clearly shows the exponential tail (figure 10d) expected at large times. This test rules out Type-I intermittency, for which $P(L)$ increases at longer times, and confirms the Type-II intermittency route to chaos in the present study.

Recent theoretical attempts to explain rheochaos treat our systems as nematogenic fluids, and consider the spatio-temporal evolution of the shear stress associated with the nematic order parameter. These models, while ignoring the complexities of breakage, flexibility and branching, capture the essential flow-induced orientability of worm-like micelles [17]. Light scattering measurements in the VH geometry are sensitive to orientational fluctuations while VV geometry is influenced by concentration and orientational order fluctuations. We describe below the results of these measurements.

SALS measurements were done with VV polarisation for half the duration and VH polarisation for remaining half of the stress relaxation run [30]. The appearance

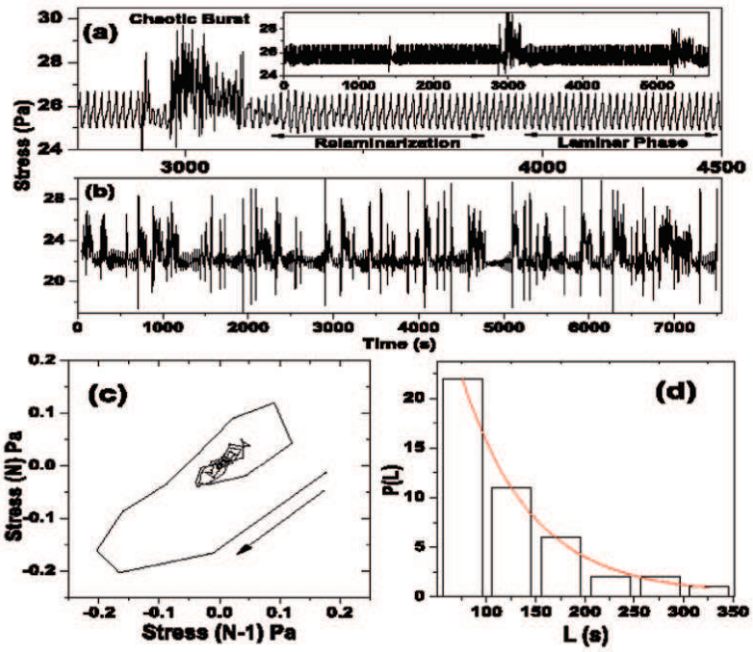

Figure 10. (**a**) Partial stress time series for CTAT 2 wt% + 100 mM NaCl at $\dot{\gamma} = 22$ s^{-1} for a different run. Inset: Full time series. (**b**) Complete stress time series for CTAT 2 wt% + 50 mM NaCl at $\dot{\gamma} = 19$ s^{-1}. (**c**) First return Poincaré plot for (a). The arrow shows the spiraling direction. (**d**) Probability distribution of laminar lengths between bursts for (b). The line is an exponential fit [30].

of an anisotropic VH scattering pattern in our SALS measurements (figure 6b(iv)) at the onset of shear-thinning implies that our systems are nematic. The time series for VV and VH intensities at a fixed wave vector, $q = 0.75$ μm^{-1}, are shown in figures 11a, b and c. Figures 11a and 11b show the time series of VV and VH intensities obtained during the stress relaxation measurement shown in figure 7a. Qualitatively, the VH intensity follows oscillations in the stress whereas VV does not. A power spectrum of the VH time series shows that the two primary frequency components (ω_1, ω_2) coincide with those obtained from the stress time series. The frequency components at $\omega_2 - \omega_1$ and $\omega_1 + \omega_2$ shown in figure 8d for the stress are absent. This may be due to the averaging procedure we have used to remove CCD noise. Figure 11c shows the VH time series for $\dot{\gamma} = 25$ s^{-1}. This time series captures the quasiperiodicity as well the chaotic burst seen in the corresponding stress relaxation measurement (figure 6b). At higher shear rates the VH time series was chaotic. We also observe that the entire VH profile shows periodic breathing patterns for $\dot{\gamma} = 23$ s^{-1} and $\dot{\gamma} = 25$ s^{-1}. This has been quantified by measuring the anisotropy (ε_s) and the orientation angle (χ_s) obtained from the second moment tensor of $S_{VH}(q,t)$ given by [36]

$$\varepsilon_s = [(\langle XX\rangle - \langle YY\rangle)^2 + 4\langle XY\rangle^2]^{1/2} \tag{2}$$

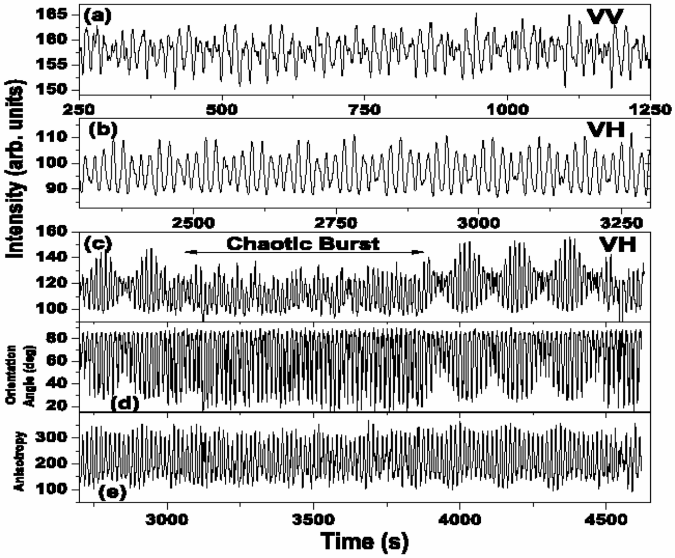

Figure 11. The VV intensity time series (**a**) and the VH intensity time series (**b**) for CTAT 2 wt% + 100 mM NaCl at $\dot{\gamma} = 23\ \mathrm{s}^{-1}$. Experiment was done with VV polarisation to the left of the break shown in the stress time series (figure 2a) and with VH polarisation to the right. (**c**) The VH intensity time series at $\dot{\gamma} = 25\ \mathrm{s}^{-1}$ (see figure 2b). (**d**) and (**e**) show the anisotropy and the orientation angle of $S_{\mathrm{VH}}(q,t)$ for (c) [30].

and

$$\tan(2\chi_{\mathrm{s}}) = \frac{2\langle XX\rangle}{\langle XX\rangle - \langle YY\rangle}, \tag{3}$$

where $\langle XY\rangle = \int \mathrm{d}q\, q_X q_Y S_{\mathrm{VH}}(q,t), \langle XX\rangle = \int \mathrm{d}q\, q_X\, q_X S_{\mathrm{VH}}(q,t)$ and $\langle YY\rangle = \int \mathrm{d}q\, q_Y\, q_Y S_{\mathrm{VH}}(q,t)$. Figures 11d and 11e show the time series of the anisotropy and orientation angle at $\dot{\gamma} = 25\ \mathrm{s}^{-1}$. The anisotropy and the orientation angle of the major axis of $S_{\mathrm{VH}}(q,t)$, which is a measure of the instantaneous orientation of the nematics, seems to follow the stress oscillations (figure 6b). The orientation angle shows regular oscillations from $\sim 20^\circ$ to $\sim 80^\circ$ when the system is in the laminar/quasiperiodic region and shows no periodicity when the system shows a chaotic burst.

To summarize, we have shown for the first time, intermittency in stress relaxation dynamics for the systems that show coupling between flow and concentration. We have also shown that the VH intensity at a fixed wave vector, anisotropy and the orientation angle shows dynamics similar to the dynamics seen in stress oscillations. In all our experiments, the 'Butterfly' pattern is always accompanied by intermittency in stress dynamics. We believe it is essential to have flow-concentration coupling to observe the rich dynamics we have seen since, this could provide a mechanism by which mechanical shear banding instabilities could cross over to shear induced demixing instabilities. The model by Rienacker *et al* [14] predicts

both temporal intermittency as well as period-doubling behaviour, in different parts of the phase diagram, for various components of the alignment tensor. To the best of our knowledge, there are no theoretical models that predict temporal intermittency in the stress for worm-like micelles that show shear banding. Interestingly, in the rheochaos model by Fielding and Olmsted [16], spatio-temporal intermittent behaviour is seen for moderate to strong coupling strength between the flow and the micellar length. Spatio-temporal intermittency route to chaos has also been predicted by [17]. A complete theoretical understanding for temporal intermittent behaviour in systems that show flow-concentration coupling is lacking at the moment. Our experiments further reinforce the case that rheochaos, far from being mere irregularity in the flow of a complex fluid, lies squarely in the domain of chaotic nonlinear dynamical systems. We hope that our results will motivate further experiments and theoretical modeling.

Acknowledgements

We would like to acknowledge fruitful discussions with Prof. Sriram Ramaswamy and Prof. M E Cates.

References

[1] P G deGennes, *Rev. Mod. Phys.* **64**, 645 (1992)
[2] T A Witten, *Rev. Mod. Phys.* **71**, S367 (1999)
[3] P N Pusey, in *Colloidal suspensions, liquids, freezing and the glass transition* (Elsevier Science Publishers B.V., 1991) p. 768
[4] A K Sood, in *Solid state physics* edited by H Ehrnrich and D Turnbull, (Academic, New York, 1991) vol. 45
[5] C W Macosko, in *Rheology: Principles, measurements and applications* (VCH Publishers, New York, 1993)
[6] J N Israelachivilli, in *Physics of amphiphiles: Micelles, vesicles and micoemuslions* edited by V Degiorgio and M Corti (North Holland, Amsterdam, 1985) pp. 23–57
[7] M E Cates and S J Candau, *J. Phys. Condens. Matter* **2**, 5869 (1990)
[8] J F A Soltero, J E Puig, O Manero and P C Schulz, *Langmuir* **11**, 3337 (1995)
[9] A K Sood, R Bandyopadhyay and G Basappa, *Pramana – J. Phys.* **53**, 223 (1999)
[10] N A Spenley, M E Cates and T C B Mcleish, *Phys. Rev. Lett.* **71**, 939 (1993)
[11] R Bandyopadhyay, G Basappa and A K Sood, *Phys. Rev. Lett.* **84**, 2022 (2000)
[12] The TISEAN package is written by R Hegger, H Kantz and T Scrieber and is publicly available at http://www.mpipks-dresden.mpg.de/∼tisean
[13] M Grosso *et al*, *Phys. Rev. Lett.* **86**, 3184 (2001)
[14] G Rienacker *et al*, *Phys. Rev.* **E66**, 040702(R) (2002)
[15] D A Head *et al*, *Phys. Rev.* **E64**, 061509 (2001)
M E Cates *et al*, *Phys. Rev.* **E66**, 025202(R) (2002)
A Aradian and M E Cates, *Europhys. Lett.* **70**, 397 (2005)
[16] S M Fielding and P D Olmsted, *Phys. Rev. Lett.* **92**, 084502 (2004)
[17] B Chakrabarti *et al*, *Phys. Rev. Lett.* **92**, 055501 (2004)
M Das *et al*, *Phys. Rev.* **E71**, 021707 (2005)

M Das *et al*, *Molecular gels* edited by P Terech and R G Weiss (Kluwer Academic Press, 2005)
[18] R Bandyopadhyay and A K Sood, *Europhys. Lett.* **56**, 447 (2001)
P Fisher, *Rheol. Acta* **39**, 234 (2000)
[19] A S Wunenburger *et al*, *Phys. Rev. Lett.* **86**, 1374 (2001)
J-B Salmon *et al*, *Phys. Rev.* **E66**, 031505 (2002)
L Courbin *et al*, *Phys. Rev. Lett.* **92**, 018305 (2004)
S Lerouge, M Argentina and J P Decruppe, cond-mat/0601708
S M Fielding and P D Olmsted, cond-mat/0511233
[20] D Lootens *et al*, *Phys. Rev. Lett.* **90**, 178301 (2003)
[21] M R L'opez-Gonzalez *et al*, *Phys. Rev. Lett.* **93**, 268302 (2004)
W M Holmes *et al*, *Europhys. Lett.* **64**, 274 (2003)
J-B Salmon *et al*, *Phys. Rev.* **E68**, 051504 (2003)
[22] V Schmitt *et al*, *Phys. Rev.* **E52**, 4009 (1995)
[23] J F Berret *et al*, *Europhys. Lett.* **25**, 521 (1994)
[24] Y Pomeau and P Manneville, *Commun. Math. Phys.* **74**, 189 (1980)
[25] C Jeffries and J Perez, *Phys. Rev.* **A26**, 2117 (1982)
M Dubois *et al*, *Phys. Rev. Lett.* **51**, 1446 (1983)
J-Y Huang and J-J Kim, *Phys. Rev.* **A36**, 1495 (1987)
[26] S M Fielding and P D Olmsted, *Europhys. J.* **E11**, 65 (2003)
[27] R Bandyopadhyay and A K Sood, *Langmuir* **19**, 3121 (2003)
[28] E Helfand and G H Fredrickson, *Phys. Rev. Lett.* **62**, 2468 (1989)
S T Milner, *Phys. Rev. Lett.* **66**, 1477 (1991)
M Doi and A Onuki, *J. Phys. II (France)* **2**, 1631 (1992)
[29] I A Kadoma and J W van Egmond, *Phys. Rev. Lett.* **76**, 4432 (1996); *Phys. Rev. Lett.* **80**, 5679 (1998)
[30] Rajesh Ganapathy and A K Sood, *Phys. Rev. Lett.* (2006) (to be published)
[31] E Ott, *Chaos in dynamical systems*, 2nd edition (Cambridge University Press, Cambridge, 1993)
[32] H S Greenside *et al*, *Physica* **D5**, 322 (1984)
[33] P Berge *et al*, *Order within chaos* (Hermann, Paris, 1984)
[34] J Sacher *et al*, *Phys. Rev. Lett.* **63**, 2224 (1989)
[35] H G Schuster, *Deterministic chaos* (VCH, Weinheim, 1988)
[36] I A Kadoma and J W van Egmond, *Langmuir* **13**, 4551 (1997)